Influence of Burial Depth of Soil on Reinforced Concrete Tunnel Against the Impact and Blast Loading

K. Senthil, Keshav Saini, and Manish Kumar

Abstract Underground Tunnels are a necessary segment of the present infrastructure system. The tunnel system has become an important part of the present infrastructure all over the world. With increasing use and popularity, the underground tunnels are always prone to natural and man-made attacks. Therefore, an attempt has been made to study the response of underground tunnels against impact loading as well as blast loading for different burial depths 5, 10, and 15 cm of soil. This paper highlights the influence of burial depth over the tunnel against impact loading with the mass of impactor 104 kg. Also, the paper highlights the influence of burial depth over the tunnel against blast loading of varying masses of TNT. The experiments were performed on the underground tunnels with different burial depths 5, 10, and 15 cm of soil and measured in terms of the impact force as well as deformed profile. The simulations were conducted on a semi-circular shaped reinforced concrete tunnel with 0.5 m center to center diameter, 1.2 m of length, and 0.05 m of thickness using ABAQUS/CAE Explicit software. The constitutive behavior of concrete, steel reinforcement, and soil element are defined by using the Concrete Damaged Plasticity model, Johnson–Cook Plasticity model, and Drucker-Prager model, respectively. The simulation findings were compared to the experimental results and they were found in good agreement. The major conclusions were drawn based on the impact as well as blast loading on the underground tunnels with varying burial depths.

Keywords Underground tunnels · Burial depth · Blast loading · Impact loading · Experiment · Simulations

K. Senthil (✉) · K. Saini · M. Kumar
Department of Civil Engineering, Dr. B R Ambedkar National Institute of Technology, G.T. Road, Amritsar Bypass, Jalandhar, Punjab 144011, India
e-mail: kasilingams@nitj.ac.in

1 Introduction

Tunneling has become a critical component of today's infrastructure systems all around the world. As a result, it's become critical to ensure the tunnels' safety against any form of man-made blasting activity or any unintentional blasting events as a result, previous research on the dynamic behavior of these structures in the face of surface blast and impact loads should be investigated. The research was based on small-diameter single-track tunnels, which are more vulnerable to internal blast stress and are typical in New York City, and used the Finite Element Method. The lining Theme: Soil-Structure Interaction, Earthquake Engineering, and Computational Geo-mechanics surface was subjected to blast pressure from the explosion, which was applied using a triangle pressure-time diagram, with the elastoplasticity of the ground and lining, as well as their nonlinear interaction, taken into account in the numerical model [1]. The damage was caused by a surface explosion of a sedan, van, small delivery truck (SDT), and container carrying 227, 454, 1814, and 4536 kg of TNT charge weight, respectively, on an underground box frame tube. To simulate and monitor the propagation of the blast pressure waves into the soil, the Arbitrary Lagrangian-Eulerian (ALE) technique was used. The research should be carried out using the ANSYS/LS-DYNA program [2]. The dynamic responses of the buried tunnel at depths of 3.5, 7, 10.5, and 14 m for the surface detonation of a 1000 kg TNT charge in sandy soil. To evaluate and compare semi-ellipse, circular, and horseshoe form tunnels, the Kobe box shape sub-way tunnel was chosen as an example. The finite element software LS-DYNA was utilized to simulate and assess the project's outcome, with the second interaction due to explosion being precisely modeled [3]. Using the widely used explicit dynamic nonlinear finite element program ANSYS/LS-DYNA, analyze the dynamic responses of the operational metro tunnel in soft soil. The blast-induced wave propagation in the soil and tunnel, as well as the von Mises effective stress and acceleration of the tunnel lining, were presented, and the tunnel lining's safety was assessed using the failure criterion and a TNT charge on the ground of no more than 500 kg, and the selection of soil parameters should be given more attention to conduct a more precise analysis [4]. Drop hammer testing is used to test the deformation behavior of tunnels in rock subjected to impact loading. To establish important factors governing fracture and deformations in structural integrity, a thorough examination is conducted. The effect of cover depth and impact energy on the shallow tunnels' settlement. The study is also carried out for various rock masses of varied strength, and tunnel collapse is calculated along the tunnel length [5]. Crack speeds are not constant during crack propagation, and cracks may temporarily stop for a length of time; the greatest arrest period in this study is 227.52 s; propagation toughness is proportional to crack speeds, and arrest toughness is lower than initiation toughness. To simulate crack propagation behavior and path, numerical models were created using the finite-difference code AUTODYN. The dynamic stress intensity factors (SIFS) were calculated using the finite element code ABAQUS [6].

Based on the detailed literature review, it was observed that the investigation on the impact of TNT mass on tunnels subjected to external blast loading AND impact loading is limited. The study was focused to analyze the behavior of reinforced concrete tunnels and its constitutive modeling based on different models is discussed in Sect. 2, while detailed finite element modeling using ABAQUS software is presented in Sect. 3. Then, the impact of external blast loading for different TNT masses placing at 1 m from the top of the soil AND impact loading on the tunnel is studied in Sect. 4, followed by conclusions in Sect. 5.

2 Constitutive Modeling

The concrete damage plasticity model was used to accommodate the tunnel's constitutive behavior, which includes compressive and tensile activity. The Johnson-cook model has been used to incorporate the elastic and plastic behavior of steel reinforcement bars, which includes the effects of state of stress, temperature, and strain rate, and is discussed in this section.

2.1 Johnson–Cook Model for Reinforcement

In the modeling of the finite element available in ABAQUS, the action of the steel deformation was computed using the Johnson-Cook model. According to strain hardening, strain rate hardening, and thermal softening, the Johnson-Cook model is a function of von Mises tensile flow stress. The Johnson-cook model is represented by Eq. (1):

$$\overline{\sigma} = \left[A + B\left(\overline{\varepsilon}^{\mathrm{pl}}\right)^2 \right] \left[1 + C \ln\left(\frac{\dot{\overline{\varepsilon}}^{\mathrm{pl}}}{\dot{\varepsilon}_0}\right) \right] \left(1 - \hat{\theta}^m\right) \tag{1}$$

where A, B, C, m, and n are material parameters, $\overline{\varepsilon}^{\mathrm{pl}}$ is equivalent plastic strain, $\dot{\overline{\varepsilon}}^{\mathrm{pl}}$ is corresponding plastic strain rate, $\dot{\varepsilon}_0$ is a reference strain rate, and $\hat{\theta}^m$ is nondimensional temperature. The material parameter at melting temperature 1800 K, transition temperature 293 K, reference strain 0.0005, and others are shown in Table 1.

Table 1 Johnson–cook model parameters for steel Fe420

A (Mpa)	B (Mpa)	C	n	m
493	383	0.0114	0.45	0.94

Table 2 Response of concrete to uniaxial loading in **a** compression, **b** tension

Concrete compression damage		Concrete tension damage	
Damage parameter	Inelastic strain	Damage parameter	Cracking strain
0	0	0	0
0.2	0.0011	0.5	0.003
0.5	0.004	0.55	0.005
–	–	0.61	0.007
–	–	0.67	0.01

2.2 Concrete Damaged Plasticity Model

The concrete damage model is a continuum, plasticity-based model. Tensile cracking and compressive crushing of the concrete material are assumed to be the two main failure causes. As indicated in Table 2, the model assumes that the uniaxial tensile and compressive response of concrete is defined by damaged plasticity.

The stress–strain response under uniaxial tension follows a linear elastic relationship until the failure stress, σ_{t_0} is achieved. The development of micro-cracking in the concrete material corresponds to the failure stress. The production of micro-cracks is reflected macroscopically by a softening stress–strain response, which promotes strain localization in the concrete structure, in addition to the failure stress. The response to uniaxial compression is linear until the initial yield value, $\sigma c0$, the response in the plastic regime is usually characterized by stress hardening followed by strain softening beyond the ultimate stress, σcu. This representation, although somewhat simplified, captures the main features of the response of concrete.

If E_0 is the material's initial (unaffected) elastic stiffness, the stress-strain relationships under uniaxial tension and compression loading are:

$$\sigma_t = (1 - d_t) E_0 \left(\varepsilon_t - \tilde{\varepsilon}_t^{pi} \right) \tag{2}$$

$$\sigma_c = (1 - d_c) E_0 \left(\varepsilon_c - \tilde{\varepsilon}_c^{pi} \right) \tag{3}$$

where the tension and compression damage variables are denoted by dt and dc, respectively. The concrete material properties for the M25 grade were taken from Keshav Saini [7]. As shown in Table 3.

2.3 Finite Element Modeling

The reinforced concrete tunnel and soil finite element model were completed by ABAQUS. The dimension of the semi-cylindrical tunnel is taken as the length of the tunnel is 1.2 m, center to center diameter of 0.5 m, and thickness of 0.05 m in concrete

Table 3 Material constants for concrete material

Density (kg/m^3)	2400
Young's Modulus (N/m^2)	2.66×10^{10}
Poisson's ratio	0.2
Dilation angle	30
Eccentricity(m)	1
K	0.66
fb0/fc0	1.16

tunnel modeling as shown in Fig. 1a. A layer of 6 mm in diameter longitudinal and transverse steel reinforcement mounted at 60 mm center to center gap as shown in Fig. 1b. The geometry of the concrete tunnel, soil, and reinforcing steel was modeled correspondingly as solid deformable and deformable wire. The crater for the external blast is located 1 m above the top of the soil. The exterior boundary of the soil element was defined by an acoustic medium with a bulk density of 1500 MPa and a density of 110 Kg/m3. The CONWEP model with the AIR BLAST concept is used to describe the origin of TNT blast load.

At the crown of the tunnel, the stress concentration was high, so fine meshing of size 0.0075 m was used whereas in the rest parts of the tunnel, global seeding of size 0.01 m was introduced. The meshing of soil was done using global seeding of size 0.05 m, mesh size of 0.02 m was provided for both longitudinal and transverse reinforcement. The acceleration due to the gravity of 9.81 m/s^2 was applied to the whole element except acoustic medium where for skin, the boundary condition is fixed in all directions.

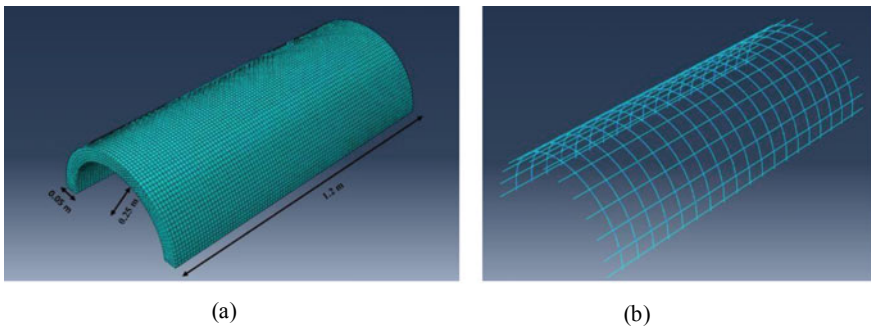(a)   (b)

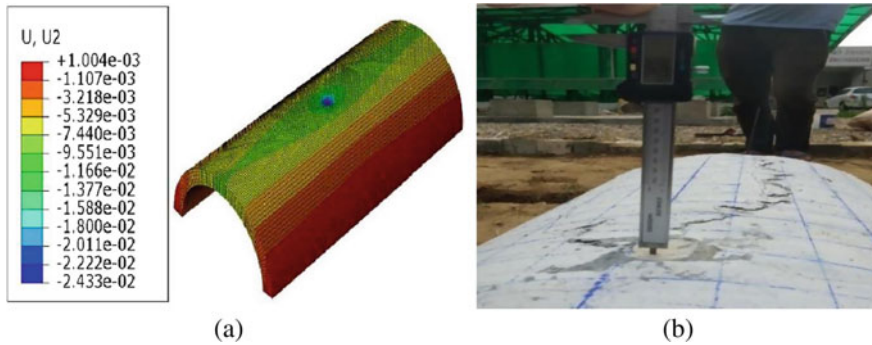**Fig. 1** Mesh modeling of **a** tunnel and **b** reinforcement

Fig. 2 Downward displacement obtained by **a** numerical simulation and **b** experimentally

2.4 Finite Element Results Validation

The experiment was carried out in a tunnel with a semi-circular cross-section with 1.2 m length, 0.5 m center to center diameter, and 0.05 m lining thickness, by falling a 104 kg hemispherical impactor from a height of 2.4 m over the tunnel [8]. The results have been recorded in terms of down-wards displacement, tension, and compression damage zone on the tunnel based on the experimental observations, as shown in Fig. 2. Overall, the numerical results accurately anticipated the region of tension and compression damage on the tunnel throughout the time step and were shown to be in good agreement with the actual results.

It was observed that a maximum deviation of 15% has been observed between the values of actual displacement and the foreseen displacement. Hence, the considered finite element model is accurate and effective.

3 Results and Discussions

The simulations were carried out for different masses of TNT placed 1 m above the center of burial soil at different burial depths of the tunnel. The tunnel was analyzed by placing TNT at 1 m from the top of the soil.

3.1 Von Mises Stresses for 0.05 m of Burial Depth

The stresses observed in the tunnel, having TNT 1 kg, were 8.5 MPa, 7.8 MPa, and 7.8 MPa at a time of 0.02, 0.035, and 0.05 s, respectively. Similarly, for 5 kg of TNT, at the same times as that for 1 kg were 15 MPa, 16.2 MPa, and 15.2 MPa, respectively, and that for 10 kg of TNT, were 17.7 MPa, 17.4 MPa, and 16.5 MPa, respectively. It
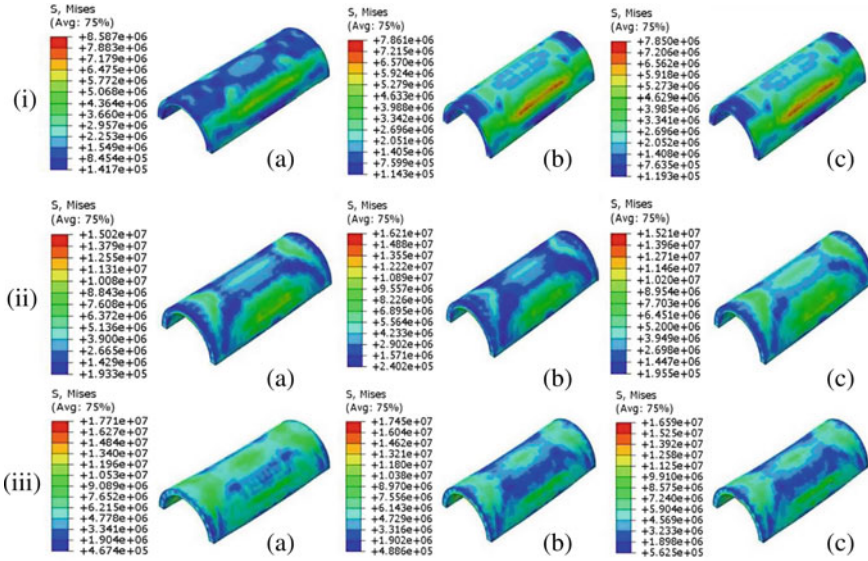
Fig. 3 Von Mises stresses for (i) 1 kg, (ii) 5 kg, (iii) 10 kg and (**a**) 0.02 s, (**b**) 0.035 s and (**c**) 0.05 s with 0.05 m burial depth

was seen that the stresses developed in the tunnel were increasing with the increase in the mass of TNT. For the rest times, comparatively higher stresses were developed when 10 kg TNT was used. Contour plots for different masses of TNT are presented in Fig. 3.

3.2 Von Mises Stresses for 0.1 m of Burial Depth

The stresses observed in the tunnel, having TNT 1 kg, were 7.9 MPa, 7.6 MPa, and 7.4 MPa at a time of 0.02, 0.035, and 0.05 s, respectively. Similarly, for 5 kg of TNT, at the same times as that for 1 kg were 14.5 MPa, 14.4 MPa, and 14.4 MPa, respectively, and that for 10 kg of TNT, were 18.2 MPa, 17.9 MPa, and 17.3 MPa, respectively. It was seen that the stresses developed in the tunnel were increasing with the increase in the mass of TNT. For the rest times, comparatively higher stresses were developed when 10 kg TNT was used. Contour plots for different masses of TNT are presented in Fig. 4.
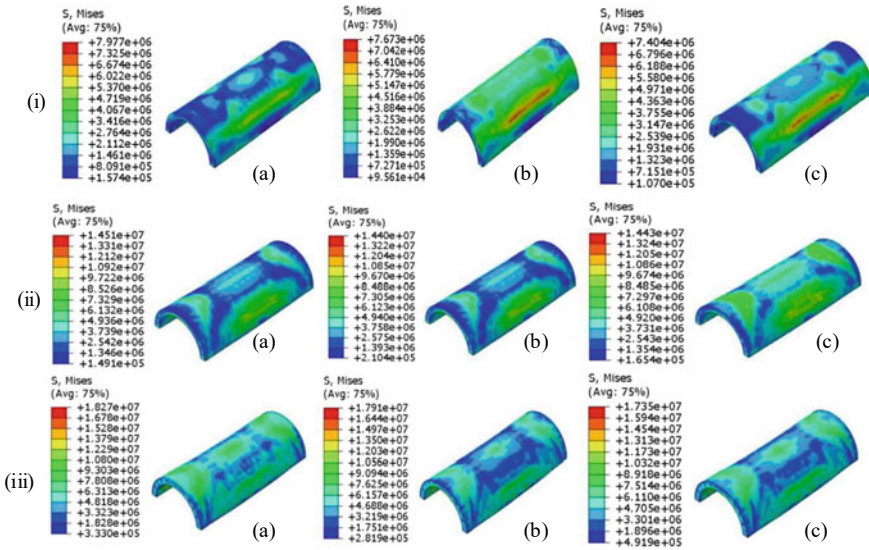
Fig. 4 Von Mises stresses for (i) 1 kg, (ii) 5 kg, (iii) 10 kg and (**a**) 0.02 s, (**b**) 0.035 s and (**c**) 0.05 s with 0.1 m burial depth

3.3 Von Mises Stresses for 0.15 m of Burial Depth

The stresses observed in the tunnel, having TNT 1 kg, were 7.6 MPa, 6.9 MPa, and 7.3 MPa at a time of 0.02, 0.035, and 0.05 s, respectively. Similarly, for 5 kg of TNT, at the same times as that for 1 kg were 15 MPa, 15 MPa, and 15.1 MPa, respectively, and that for 10 kg of TNT, were 17.6 MPa, 17.5 MPa, and 17.5 MPa, respectively. It was seen that the stresses developed in the tunnel were increasing with the increase in the mass of TNT. For the rest times, comparatively higher stresses were developed when 10 kg TNT was used. Contour plots for different masses of TNT are presented in Fig. 5.

3.4 Von Mises Stresses for Impact Loading of 104 kg

The stresses observed in the tunnel, having the weight of 104 kg of impactor at a burial depth of 0.05 m, were 25.5 MPa, 14.6 MPa, and 15.17 MPa at a time of 0.02, 0.035, and 0.05 s, respectively. Similarly, for 0.1 m of burial depth, at the same times as that for 5 cm, burial depth was 73.2 MPa, 18.9 MPa, and 19.4 MPa, respectively, and that for 0.15 m burial depth, were 19 MPa, 72.7 MPa, and 75.9 MPa, respectively. It was seen that the stresses developed in the tunnel were increasing with increase burial depth. Contour plots for different burial depths are presented in Fig. 6.
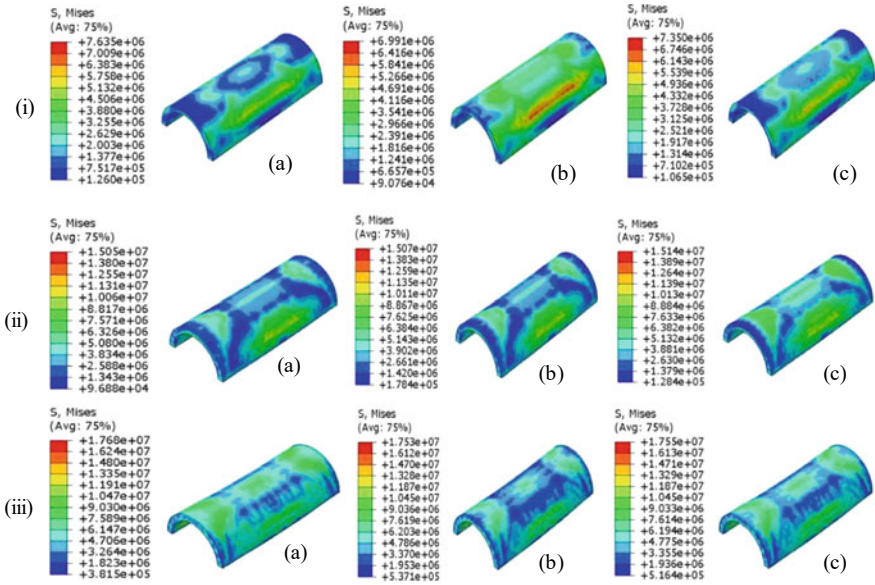
Fig. 5 Von Mises stresses for (i) 1 kg, (ii) 5 kg, (iii) 10 kg and (**a**) 0.02 s, (**b**) 0.035 s and (**c**) 0.05 s with 0.15 m burial depth
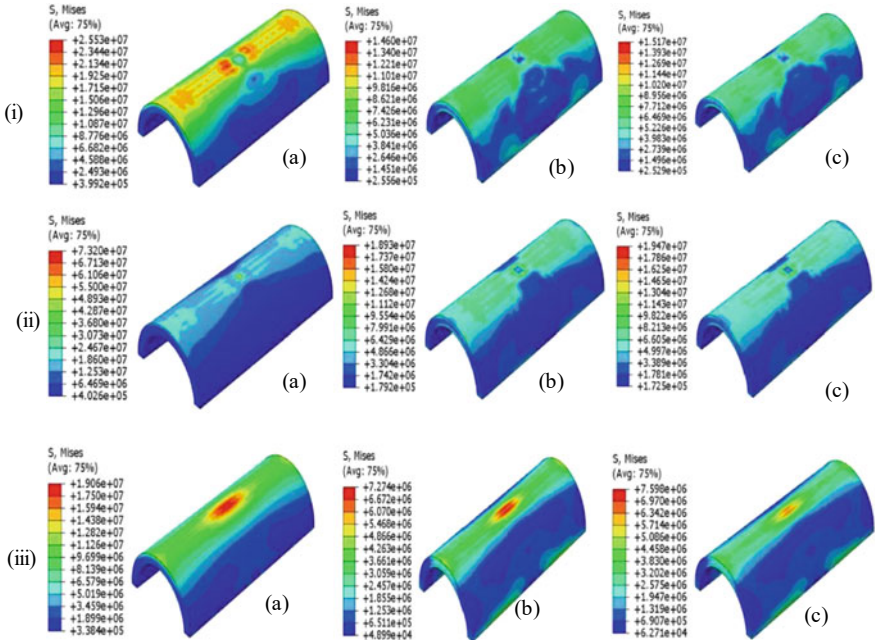

Fig. 6 Von Mises stresses for (i) 5 cm, (ii) 10 cm, (iii) 15 cm and (**a**) 0.02 s, (**b**) 0.035 s and (**c**) 0.05 s against 104 kg mass of impactor

4 Displacement

The displacement observed in the tunnel, at Burial Depth (BD) 0.05 m having TNT 1 kg, was maximum displacement 3.26 mm, respectively. Similarly, for 5 kg were 14.703 mm, and that for 10 kg of TNT, were 23.684 mm, respectively. It was seen that the displacement in the tunnel was increasing with the increase in the mass of TNT. For the rest times, comparatively higher displacement was developed when 10 kg TNT was used. Graph plots for different masses of TNT are presented in Fig. 7a.

The displacement observed in the tunnel, at Burial Depth (BD) 0.1 m having TNT 1 kg, was maximum displacement of 3.087 mm, respectively. Similarly, for 5 kg were 18.858 mm, and that for 10 kg of TNT, was 34.9 mm, respectively. It was seen that the displacement in the tunnel was increasing with the increase in the mass of TNT. For the rest times, comparatively higher displacement was developed when 10 kg TNT was used. Graph plots for different masses of TNT are presented in Fig. 7b.

The displacement observed in the tunnel, at Burial Depth (BD) 0.15 m having TNT 1 kg, was maximum displacement 3.05 mm, respectively. Similarly, for 5 kg
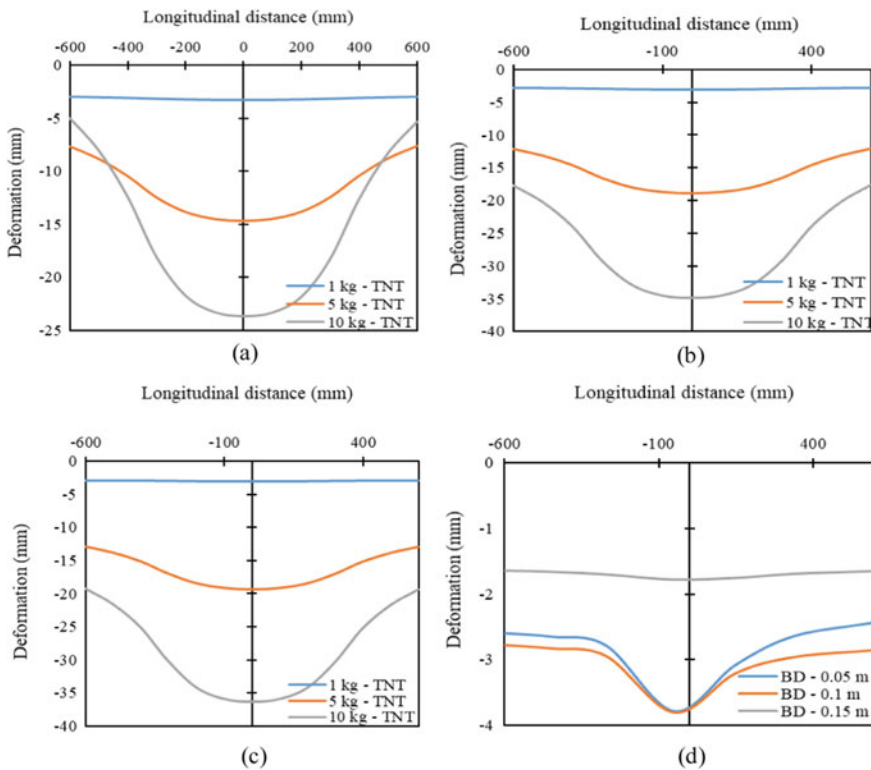

Fig. 7 Vertical downward displacements for burial depth (**a**) 0.05 m (**b**) 0.1 m (**c**) 0.15 m at different TNT masses and (**d**) impact load at different burial depth

were 19.403 mm, and that for 10 kg of TNT, were 36.332 mm, respectively. It was seen that the displacement in the tunnel was increasing with the increase in the mass of TNT. For the rest times, comparatively higher displacement was developed when 10 kg TNT was used. Graph plots for different masses of TNT are presented in Fig. 7c.

The displacement observed in the tunnel, having the weight of 104 kg of impactor at a burial depth of 0.05 m, was a maximum displacement of 3.79 mm. Similarly, for 10 cm of burial depth were 3.81 mm, respectively, and that for 15 cm burial depth, were 1.79 mm, respectively. It was seen that the displacement in the tunnel was decreased with increase burial depth. Contour plots for different burial depths are presented in Fig. 7d.

The displacement observed in the tunnel at the center node, at Burial Depth (BD) 0.05 m having TNT 1 kg, were maximum displacement 5.284 mm, respectively. Similarly, for 5 kg was 27.927 mm, and that for 10 kg of TNT, were 57.359 mm, respectively. It was seen that the displacement in the tunnel was increasing with the increase in the mass of TNT. For the rest times, comparatively higher displacement was developed when 10 kg TNT was used. Graph plots for different masses of TNT are presented in Fig. 8a.

The displacement observed in the tunnel at the center node, at Burial Depth (BD) 0.1 m having TNT 1 kg, were maximum displacement 5.086 mm, respectively. Similarly, for 5 kg were 26.7 mm, and that for 10 kg of TNT, were 53.7855 mm, respectively. It was seen that the displacement in the tunnel was increasing with the increase in the mass of TNT. For the rest times, comparatively higher displacement was developed when 10 kg TNT was used. Graph plots for different masses of TNT are presented in Fig. 8b.

The displacement observed in the tunnel at the center node, at Burial Depth (BD) 0.15 m having TNT 1 kg, were maximum displacement 4.995 mm, respectively. Similarly, for 5 kg were 26.46 mm, and that for 10 kg of TNT, was 53.64 mm, respectively. It was seen that the displacement in the tunnel was increasing with the increase in the mass of TNT. For the rest times, comparatively higher displacement was developed when 10 kg TNT was used. Graph plots for different masses of TNT are presented in Fig. 8c.

The displacement observed in the tunnel at the center node, having the weight of 104 kg of impactor at a burial depth of 0.05 m, was a maximum displacement of 12.923 mm. Similarly, for 0.1 m of burial depth were 13.669 mm, respectively, and that for 0.15 m burial depth, were 5.964 mm, respectively. It was seen that the displacement in the tunnel was decreased with increase burial depth. Contour plots for different burial depths are presented in Fig. 8d.

5 Acceleration

The acceleration observed at the center node in the tunnel having burial depth of 0.05 m, having TNT 1 kg, was maximum acceleration of 5774.82 m/s², respectively.
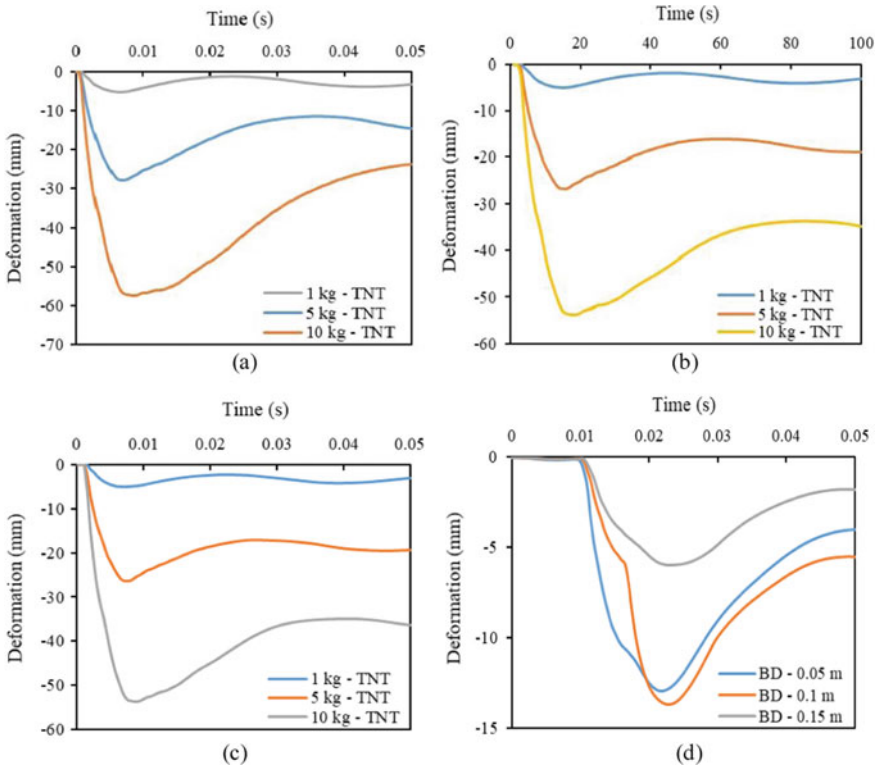
Fig. 8 Vertical downward displacements at center node for burial depth **a** 0.05 cm **b** 0.1 cm **c** 0.15 m at different TNT masses and **d** impact load at different burial depths

Similarly, 5 kg of TNT was a maximum of 15659.7 m/s^2, and that for 10 kg of TNT, was a maximum of 42149 m/s^2, respectively. It was seen that the acceleration in the tunnel was increasing with the increase in the mass of TNT. For the rest times, comparatively maximum acceleration was developed when 10 Kg TNT was used. Graph plots between time versus acceleration are presented in Fig. 9a. The acceleration observed at the center node in the tunnel having burial depth of 0.1 m, having TNT 1 kg, was maximum acceleration of 7644.69 m/s^2, respectively. Similarly, 5 kg of TNT were maximum 35142.7 m/s^2 and that for 10 kg of TNT, were maximum 55039.7 m/s^2, respectively. It was seen that the acceleration in the tunnel was increasing with the increase in the mass of TNT. For the rest times, comparatively maximum acceleration was developed when 10 kg TNT was used. Graph plots between time versus acceleration are presented in Fig. 9b.

The acceleration observed at the center node in the tunnel having burial depth of 0.15 m, having TNT 1 kg, was maximum acceleration 7461.64 m/s^2, respectively. Similarly, 5 kg of TNT was a maximum of 6994.83 m/s^2, and that for 10 kg of TNT, was a maximum of 18559.9 m/s^2, respectively. It was seen that the acceleration in the tunnel was increasing with the increase in the mass of TNT. For the rest
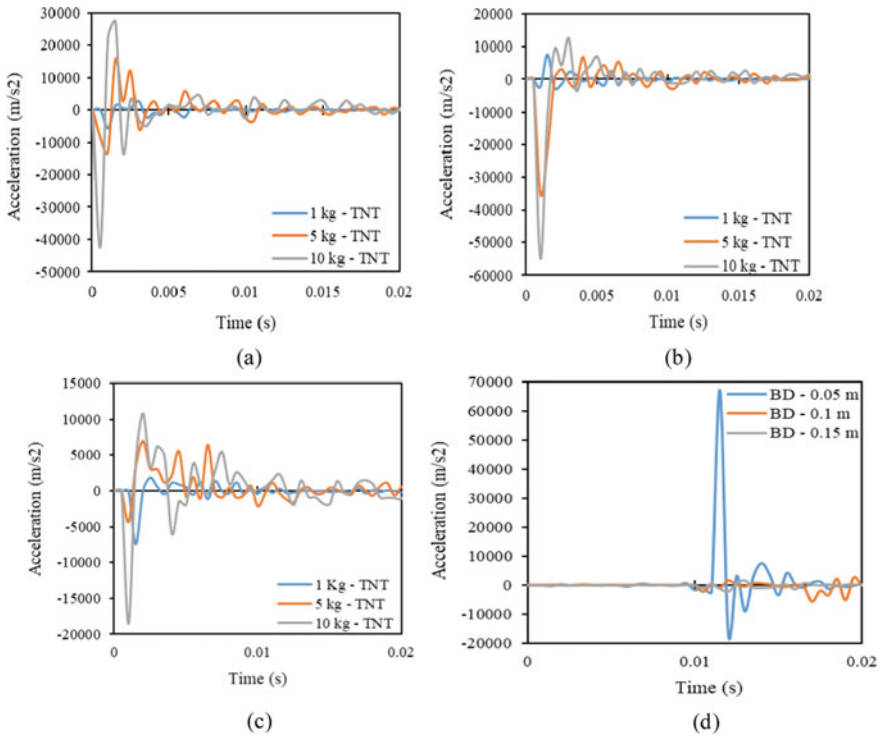
Fig. 9 Vertical accelerations at center node for burial depth (**a**) 0.05 m (**b**) 0.1 m (**c**) 0.15 m at different TNT masses and (**d**) impact load at different burial depth

times, comparatively maximum acceleration was developed when 10 kg TNT was used. Graph plots between time versus acceleration are presented in Fig. 9c. The acceleration observed at the center node in the tunnel, having the weight of 104 kg of impactor at a burial depth of 0.05 m, was maximum acceleration 67021.2 m/s^2, respectively. Similarly, for burial depth 0.1 m were maximum 17393.3 m/s^2, and that for burial depth 0.15 m, were maximum 2102.45 m/s^2, respectively. It was seen that the acceleration in the tunnel was decreased with an increase in the burial depth of soil. For the rest times, comparatively maximum acceleration was developed at a 0.05 m burial depth graph plots between time versus acceleration are presented in Fig. 9d.

Longitudinal, node deformation and acceleration in the tunnel increase with increase mass of TNT for a burial depth. Longitudinal, node deformation and acceleration in the tunnel decrease with an increase in burial depth for impact loading shown in Table 4.

Table 4 Peak longitudinal, node displacement and acceleration on the tunnel with varying burial depth

Specimen no		Peak displacement		Peak acceleration (m/s^2)
		Longitudinal deformation (mm)	Node deformation (mm)	
BD-0.05 m	1 kg-TNT	3.26	5.284	5774.82
	5 kg-TNT	14.703	27.927	15,659.7
	10 kg-TNT	23.684	57.359	42,149
BD-0.10 m	1 kg-TNT	3.087	5.086	7644.69
	5 kg-TNT	18.858	26.7	35,142.7
	10 kg-TNT	34.9	53.7855	55,039.7
BD-0.15 m	1 kg-TNT	3.05	4.995	7461.64
	5 kg-TNT	19.403	26.46	6994.83
	10 kg-TNT	36.332	53.64	18,559.9
Impact loading	BD-0.05 m	3.79	12.923	67,021.2
	BD-0.1 m	3.81	13.669	17,393.3
	BD-0.15 m	1.79	5.9644	2102.45

6 Conclusion

The following conclusions were obtained based on the extensive investigations:

- It was observed that the Von Mises stresses developed in the tunnel increase with increase mass of TNT for a burial depth and decrease with increase with burial depth for a TNT mass.
- The longitudinal deformation in the tunnel increase with increase mass of TNT for a burial depth, and node deformation also increases with increase mass of TNT for a burial depth.
- It was concluded that the acceleration in the tunnel increase with increase mass of TNT for a burial depth.
- It was also concluded that the deformation in the tunnel decrease with an increase in burial depth for impact loading.
- The acceleration in the tunnel decrease with an increase in burial depth for impact loading.

References

1. Liu H (2009) Dynamic analysis of subway structures under blast loading. Geotech Geol Eng 27(6):699–711
2. Zaid M (2021) Preliminary study to understand the effect of impact loading and rock weathering in tunnel constructed in quartzite. Geot Geol Eng

3. Tiwari R, Chakraborty T, Matsagar V (2017) Dynamic analysis of tunnel in soil subjected to internal blast loading. Geotech Geol Eng 35(4):1491–1512
4. Xiang Y, Yang Y (2017) Spatial dynamic response of submerged floating tunnel under impact load. Mar Struct 53:20–31
5. Gahoi, Zaid M, Mishra S, Rao KS (2017) Numerical analysis of the tunnels subjected to impact loading
6. Zhou L, Zhu Z, Wang M, Ying P, Dong Y (2018) Dynamic propagation behavior of cracks emanating from tunnel edges under impact loads. Soil Dyn Earthq Eng (August 2017)
7. Saini K (2021) MTech Thesis, National Institute of Technology, Jalandhar
8. Hafezolghorani M, Hejazi F, Vaghei R, Jaafar MSB, Karimzade K (2017) Simplified damage plasticity model for concrete. Struct Eng Int